crystals

MDPI

Article

Analysis of Multi-Hit Crystals in Serial Synchrotron Crystallography Experiments Using High-Viscosity Injectors

Marjan Hadian-Jazi [1,2,3], Peter Berntsen [1], Hugh Marman [1], Brian Abbey [1] and Connie Darmanin [1,*]

[1] Australian Research Council (ARC) Centre of Excellence in Advanced Molecular Imaging, Department of Chemistry and Physics, La Trobe Institute for Molecular Sciences, La Trobe University, Bundoora, VIC 3086, Australia; m.hadianjazi@latrobe.edu.au (M.H.-J.); p.berntsen@latrobe.edu.au (P.B.); hjmarman@students.latrobe.edu.au (H.M.); b.abbey@latrobe.edu.au (B.A.)

[2] Australian Nuclear Science and Technology Organisation (ANSTO), Lucas Heights, NSW 2234, Australia

[3] European XFEL GmbH, Holzkoppel 4, 22869 Schenefeld, Germany

* Correspondence: c.darmanin@latrobe.edu.au

Abstract: Serial Synchrotron Crystallography (SSX) is rapidly emerging as a promising technique for collecting data for time-resolved structural studies or for performing room temperature micro-crystallography measurements using micro-focused beamlines. SSX is often performed using high frame rate detectors in combination with continuous sample scanning or high-viscosity or liquid jet injectors. When performed using ultra-bright X-ray Free Electron Laser (XFEL) sources serial crystallography typically involves a process known as 'diffract-and-destroy' where each crystal is measured just once before it is destroyed by the intense XFEL pulse. In SSX, however, particularly when using high-viscosity injectors (HVIs) such as Lipidico, the crystal can be intercepted multiple times by the X-ray beam prior to exiting the interaction region. This has a number of important consequences for SSX including whether these multiple-hits can be incorporated into the data analysis or whether they need to be excluded due to the potential impact of radiation damage. Here, we investigate the occurrence and characteristics of multiple hits on single crystals using SSX with lipidico. SSX data are collected from crystals as they tumble within a high viscous stream of silicone grease flowing through a micro-focused X-ray beam. We confirmed that, using the Eiger 16M, we are able to collect up to 42 frames of data from the same single crystal prior to it leaving the X-ray interaction region. The frequency and occurrence of multiple hits may be controlled by varying the sample flow rate and X-ray beam size. Calculations of the absorbed dose confirm that these crystals are likely to undergo radiation damage but that nonetheless incorporating multiple hits into damage-free data should lead to a significant reduction in the number of crystals required for structural analysis when compared to just looking at a single diffraction pattern from each crystal.

Keywords: high-viscosity injectors; serial crystallography; synchrotron; micro-crystallography; time resolve crystallography

check for updates

Citation: Hadian-Jazi, M.; Berntsen, P.; Marman, H.; Abbey, B.; Darmanin, C. Analysis of Multi-Hit Crystals in Serial Synchrotron Crystallography Experiments Using High-Viscosity Injectors. *Crystals* **2021**, *11*, 49. https://doi.org/10.3390/cryst11010049

Received: 16 October 2020
Accepted: 6 January 2021
Published: 9 January 2021

Publisher's Note: MDPI stays neutral with regard to jurisdictional claims in published maps and institutional affiliations.

Copyright: © 2021 by the authors. Licensee MDPI, Basel, Switzerland. This article is an open access article distributed under the terms and conditions of the Creative Commons Attribution (CC BY) license (https://creativecommons.org/licenses/by/4.0/).

1. Introduction

Synchrotron-based crystallography is currently undergoing rapid development, in part driven by advances in serial femtosecond crystallography (SFX) at the XFEL. Whilst the conventional approach of measuring individual diffraction patterns from a single cryo-frozen crystal is still the most common method of structure determination, the use of SSX, particularly for time-resolved serial crystallography (TR-SX), is growing rapidly [1,2]. Whilst cryo-electron microscopy (cryo-EM) has been extremely successful for investigating the structures of molecules, any dynamic information from cryo-EM must be extracted from an analysis of dynamic unperturbed structures cryo-preserved in different conformations. Since cryo-EM provides little information regarding the nature of the perturbation that induced this polymorphism, it is of limited use in the context of studying dynamic behaviour.

This has been one of the driving motivations behind the development of methods for studying molecular dynamics in crystals at room temperature using synchrotron X-rays. Whilst serial crystallography has largely been developed at XFELs [3–9], several synchrotron facilities around the world are beginning to implement their own setups for performing SSX [10–18] with some of them having successfully demonstrated time-resolved experiments at synchrotrons [19–23]. This includes the Australian Synchrotron where serial millisecond crystallography is currently being developed using the high-viscosity Lipidico injector. For SSX to be successful, efficient sample delivery and rapid data collection are key. The methods for sample delivery for SSX currently being developed at synchrotrons can be broadly classed as either 'static' delivery systems where the crystals are rapidly scanned past the X-ray beam whilst mounted on a fixed holder or 'injector' delivery systems which involve a continuous stream of some carrier fluid or matrix past the X-ray interaction region.

The static systems include substrates, where crystals are encapsulated and data can be collected at either room temperature or under cryogenic conditions. These systems comprise a number of different setups where a series of single snapshots is generated from a large number of small crystals which are rastered through the X-ray beam [24–30].

The second type of delivery system used for SSX are injectors. The advantage of injector systems are that for room temperature measurements it is far easier to keep crystals stable and hydrated whilst embedded in a suitable matrix (e.g., buffer solution or lipid). High viscosity injectors offer the possibility to deliver crystals in a hydrated environment with minimal background. The use of liquid or gel-like matrices [31–36] opens up the possibility of performing mix-and-inject experiments where the crystal solution or slurry can be combined with a reactant immediately prior to delivery to the X-ray beam. In addition to chemical triggers, optical pulses have also proved to be enormously successful for studying the dynamics of some light activated proteins [37]. When using a low viscous carrier such as water, a liquid jet stream is formed and focussed, typically using a gas dynamic virtual nozzle (GDVN) [38–40]. However, when the rate of sample delivery can be slowed down, higher viscous media can be used to deliver crystals, such as monoolein or agarose gels. Injectors which operate with these types of samples are known as high-viscosity injectors (HVIs) and they are particularly useful for studying e.g., membrane proteins, which are often crystallised in lipidic cubic phase matrices [41]. Whilst both methods of injection have been used for serial crystallography, the slower flow rates for HVIs make them an attractive option for synchrotrons where, typically, the sample does not need to be replenished as often as for XFELs. HVIs will also normally involve lower sample consumption rates than liquid jets and can therefore be preferable in cases where the amount of crystal sample available is limited. It is for these reasons that HVIs were chosen as the primary sample delivery method of choice when developing SSX at the Australian synchrotron. However, whilst running and testing the Lipidico at the Australian synchrotron, we observed that an unexpected consequence of the slower sample delivery combined with the high frame rate using the Eiger 16M was that several single crystals were measured multiple times; whilst this is not a unique observation and is common in HVI [20], the present study specifically aids in the understanding and investigation of this important topic. The focus of this paper is analysing these multiple hits and determine their characteristics.

From our analysis, we are able to determine the maximum possible number of multiple hits, given a particular crystal size and beam diameter. We also analyse the absorbed dose per single crystal and discuss the implications for crystal consumption when performing SSX, e.g. for time-resolved structural studies.

2. Materials and Methods

2.1. Sample Preparation and Data Collection

The general setup and data analysis pipeline developed for this experiment is described in [10,42]. Briefly, lysozyme (250 mg/mL re-suspended in 50 mM sodium acetate

solution) crystals were grown using batch method in 1.5 M lithium chloride, 0.2 M sodium acetate, 40% polyethylene glycol 6000, pH 4.8. These crystals were mixed with a carrier consisting of silicone grease using a gas-tight glass syringe coupled system. The crystal size distribution range was analysed from optical microscopy data based on ImageJ [43] using particle analysis. The syringe was loaded directly on to the Lipidico injector system at the MX2 beamline at the Australian Synchrotron. The beam size was 22 × 12 µm (FWHM h × w) and the incident energy 13 keV, yielding a flux of 2.4×10^{12} photons/s. The inner diameter of the injection needle was 108 µm and the flow rate of the stream was ∼1.0 nL/s (velocity ∼100 µm/s). SSX diffraction data was collected using an EIGER X 16 M detector (running at 100 Hz).

2.2. Identification of Single Crystals Hit Multiple Times

Bragg reflections were detected using the robust peak finding method (RPF) of Hadian Jazi et al. [44] . Indexing (Mosflm and Dirax), scaling and merging of the data were carried out using CrystFel version 0.8.0 [45]. Following SSX data collection, multiple hits on a single crystal were identified via an initial screening process performed using Whirligig, a program within the CrystFel suite. The stream file used to solve the lysozyme structure [10] contained all the hits from the data. We used this file to identify which images belonged to the same crystal. This program generated a list of diffraction images where the change in crystal rotation angle between consecutive frames was less than 2 degrees, which was our estimate for the maximum value of the crystal rotation through the high-viscosity silicone grease. These images were assumed to originate from the same single crystal. As further validation, we constructed an idealised model of the beam assuming a 2D Gaussian profile of 22 µm × 12 µm (H × V). For simplicity, we assumed that the crystal was a perfect square of 12 µm ×12 µm to be consistent with the most common crystal size observed from optical characterisation data. Since the crystal can arrive in a random orientation we looked at the case of when the crystal was oriented at 0°and at 45° with respect to the horizontal beam axis. From experimental observations, to measure a diffraction signal from the crystal on the timescale of a single frame the X-ray beam needs to intersect with around 10 μm^2 of crystal. Setting this as a lower limit on the crystal size in the beam and using the convolution of the crystal and X-ray beam to determine the total possible interaction region, we find that the expected number of multiple hits varies between 6.3 and 6.5 hits/crystal for 0° and at 45° crystal tilts, respectively. This is only slightly higher than the observed multi-hit average of 6.2 hits/crystal. In addition, applying the same simple model, for the largest crystal size (35 µm) the maximum number of expected multiple hits varies between 42 and 56 for 0° and at 45° crystal tilts. Whilst this idealised model ignores factors such as background due to the LCP jet, it demonstrates that the numbers of multi-hits determined in this experiment are plausible. Finally, the time stamps of the image files were used to independently confirm that the frames were collected consecutively. These images, which were a subset of the full dataset and confirmed as originating from single crystals measured multiple times in the X-ray beam, were extracted and used to form a separate set of data we term the 'multi-hit' dataset.

2.3. Radiation Dose Calculation

The radiation dose absorbed by the crystal was calculated using the online version of RADDOSE 3D (version 3) [46] and following Marman et al. [47]; both of these calculations take into account the effects of photoelectron escape which can become noticeable as the crystal size approaches the micron scale. The absorbed dose calculations assumed a Gaussian beam profile and an angular rotation of 2 degrees. The dose calculations started from when the crystal would enter the tail of the beam and then the 2 degree rotation would occur during the total time for which the crystal interacted with the X-ray beam. The exposure time was adjusted to match this interaction time. We used a cuboid shaped crystal for the calculations and 0.42 s as the longest exposure time from our multi-hit sequence analysis on one crystal. The exposure time for three most common crystal sizes

was varied between 0 and 0.42 s with the crystal composition and surrounding solutions also incorporated into the dose calculations. We note that these calculations could be used to ensure that the multi-hit crystals remained below the radiation damage thresholds in future experiments.

3. Results

3.1. Crystal Size Distribution

The crystal size distribution (Figure 1) was generated based on analysis of optical micrographs. The size analysis showed that the cuboid lysozyme crystals ranged in their longest length 10–35 µm by 5–10 µm. However, a few outlier crystals of much larger diameter, up to 35 µm, were observed.

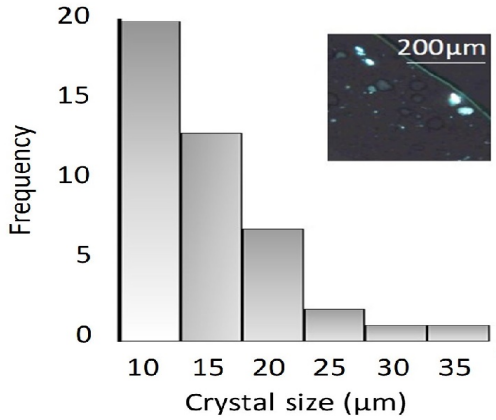


Figure 1. Size distribution of crystals in silicone grease. A small amount of sample was deposited under a cover slip and optical microscopy images of the drop were taken. The crystal size was calculated based on a single particle analysis carried out in ImageJ [43]. The insert in the upper right hand corner shows a photo of the lysozyme crystals embedded in the silicone grease.

3.2. Radiation Dose

Since these SSX measurements were conducted at room temperature, particular consideration had to be given to the effects of radiation damage. Based on calculations performed using RADDOSE 3D [46], a plot of the absorbed dose for a single crystal travelling through the X-ray beam with the maximum possible exposure time and for varying crystal sizes is shown in Figure 2. Since larger crystals can be expected to be more radiation tolerant, the number of 'damage-free' multi-hits rises in proportion with the crystal size (Figure 2A). Considering the fact that the majority of crystals measured in this experiment were between 10 and 15 µm in diameter, we do not expect that these crystals will pass through the X-ray beam without undergoing some radiation damage; this is evidenced by the high dose estimates for these crystals (Figure 2B). The amount of time that a crystal can spend in the X-ray beam prior to experiencing radiation damage was calculated to be 0.08 s for a 10 µm diameter crystal, increasing to 0.15 s for a 20 µm crystal. This was calculated based on the results in Figure 2B, where the dose threshold for lysozyme (0.38 MGy) [48] is displayed as a horizontal dotted line. Given that the detector used for these measurements was running at a frame rate of 100 Hz, this means typically between 8 and 15 diffraction images could be collected from a single crystal prior to reaching the damage threshold. Since we observe experimentally up to 42 consecutive diffraction images recorded from the same single crystal it is almost certain that, on average, a crystal will experience significant radiation damage prior to exiting the beam interaction area. This has implications when using and merging multi-hit SSX data.

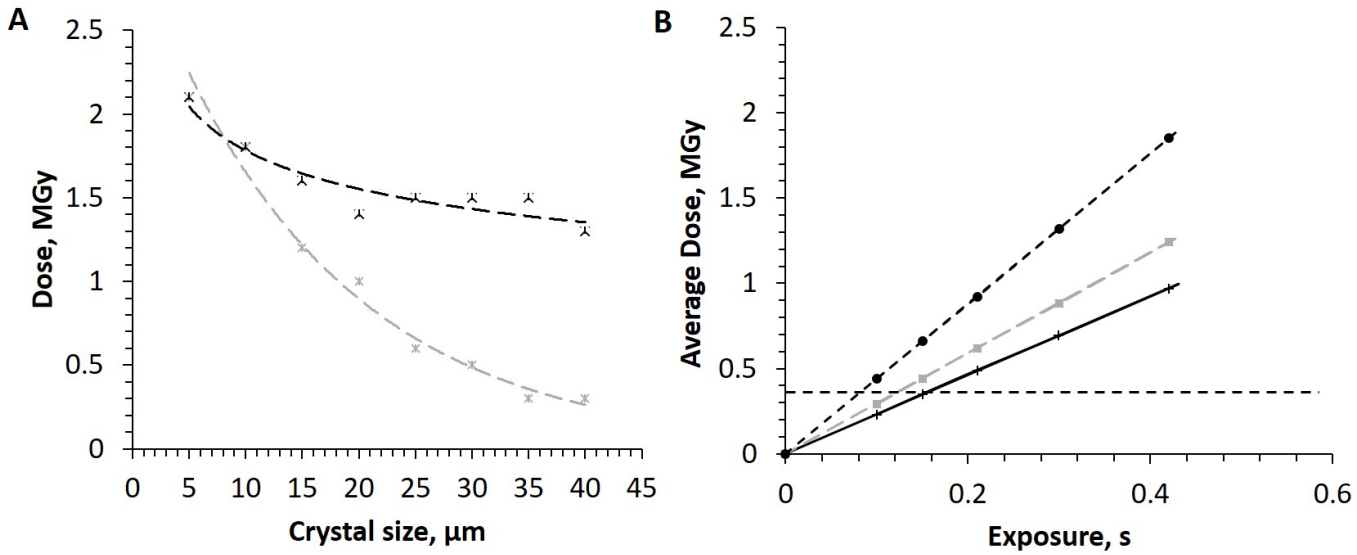


Figure 2. (**A**) Average dose received by the whole crystal (grey markers) and the average dose received by the volume of crystal interacting with the X-ray beam (black markers). The corresponding dashed lines are lines of best fit to guide the eye. (**B**) Average dose received by a whole crystal of 20 µm (black solid line), 15 µm (grey dashed line) and 10 µm (black dotted line) diameter as a function of the exposure time [40] The room temperature radiation damage limit for lysozyme is 0.38 MGy and is indicated by the horizontal black dashed line [48].

To confirm the predictions of RADDOSE 3D, the quality of diffraction patterns collected during the multi-hit SSX measurements for the 315 multi-hit crystals were analysed. Three crystals were selected as being representative of the complete multi-hit dataset. SSX diffraction patterns collected from a single crystal as it tumbles through the X-ray beam within the Lipidico sample stream are presented in Figure 3 and Movie S1 in Supplementary Materials. Visual inspection of the intensities of the Bragg peaks over Frames 1–19, for Crystal 3, does not reveal any significant decrease in diffraction quality (Movie S1); however, an examination of the peak intensities within the higher resolution shell reveals a decrease in intensity and peak number. A second crystal, Crystal 2, was also investigated with a total of 42 frames collected (Figure S1 and Movie S2). Comparison of Frames 1, 20 and 42 revealed a small but systematic decrease in the measured intensity. A similar trend was observed for a third crystal, Crystal 1, where 19 consecutive images were collected (Figure S2 and Movie S3). A closer examination of the intensities of Bragg peaks within the highest resolution shell also revealed the number of outer shell reflections decrease as well as the average intensity (Table S1). Overall, the results of the three representative crystals (out of 312 crystals which comprise the multi-hit dataset) whose consecutive frames we analysed in detail consistently indicate a fading of diffraction spots over similar timescales predicted by the dose measurements.

3.3. Model of Crystal Tumbling in the Sample Stream

Experimentally, the maximum number of consecutive multiple hits observed for a single crystal was 42. This is consistent with an X-ray beam size of 22 × 12 µm and a crystal size of 20 × 20 µm, with a flow rate of 100 µm/s, which matches the known experimental parameters. If the crystal diameter is reduced to 10 µm, the maximum possible number of achievable multiple hits for a single crystal decreases to 32. We note that the corresponding time the leading edge of the crystal enters the X-ray beam to the point at which the trailing edge of the crystal exits the X-ray beam ranges from 0.32 to 0.42 s for a crystal diameter from 10 to 20 µm. Figure 4 shows an illustration of the experimental setup and how the crystals tumble within the high viscous stream before exiting the X-ray interaction region.

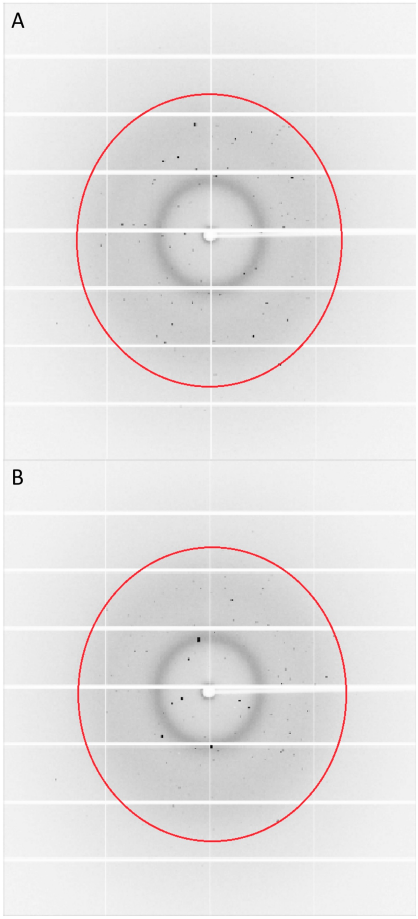


Figure 3. Diffraction images from a single crystal (Crystal 3) as it tumbles through the X-ray beam: (**A**) the first diffraction image collected, Frame 1; and (**B**) the last image collection in the series, Frame 18. The large red ring indicates the outer resolution limit of the diffraction pattern.

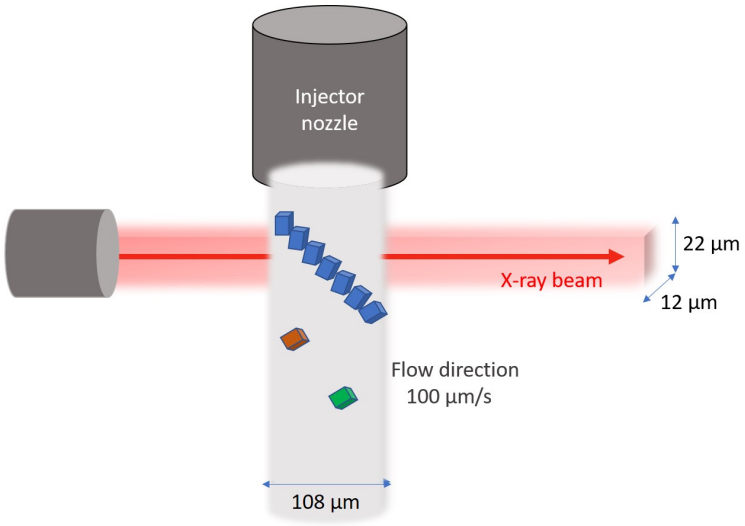


Figure 4. A schematic showing a crystal tumbling in the high viscous stream (shaded grey) as it passes through the X-ray interaction region (shaded red).

3.4. Generation of Multiple Hits on a Single Crystals

In this investigation, we created a subset of data and identified as crystals that were hit more than once as they passed through the X-ray interaction region and defined this as a 'multi-hit' dataset. Figure 5 shows the number of crystals that have been hit multiple

times. Whilst the maximum number of multi-hits on a single crystal was found to be 42, the average number of multiple hits was much lower than this, at 6.2 hits/crystal.

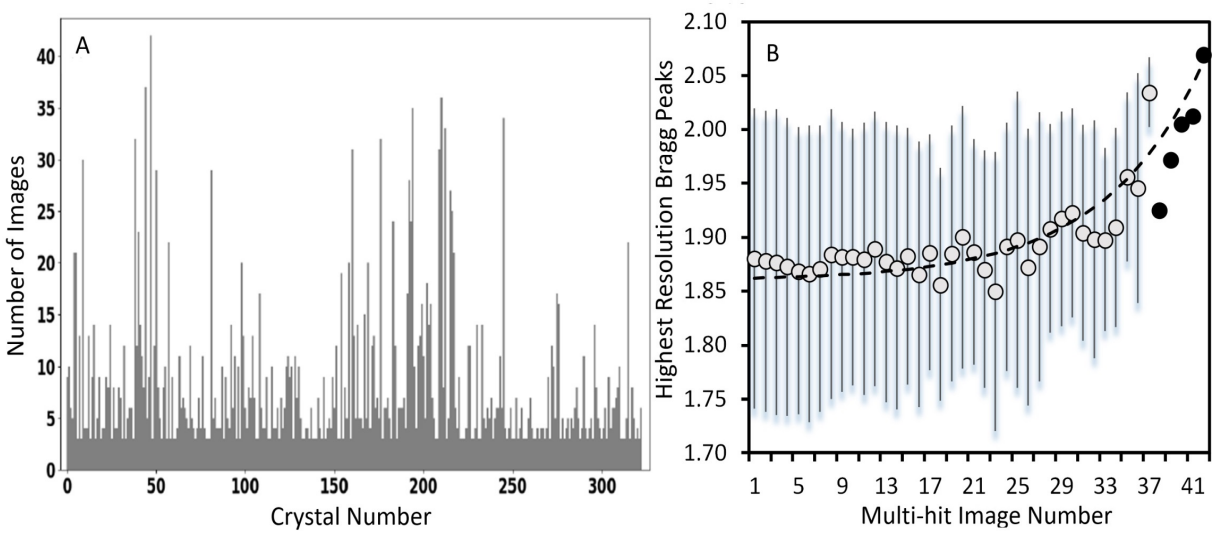


Figure 5. Multi-crystal sequence of events. (**A**) This plot shows the total number of images collected per single crystal for each of the 315 crystals that were hit multiple times as they passed through the X-ray beam. We found that the maximum number of images collected for a single multi-hit crystal was 42. (**B**) This plot shows the upper limit on the resolution of Bragg peaks indexed by the CrystFel suite in each series of frames from 1 of 42 for the 315 crystals in (A). The vertical lines reflect the standard deviation in the values for each data point. Above 37 mutli-hits, there are fewer than three data points; these points are coloured solid black.

Once the crystals with multiple hits were identified, the dataset was further analysed to generate crystallography data collection statistics (Table 1). Analysis of the complete dataset collected revealed 7.6% of the crystals used to generate the lysozyme structure (which comprised 4794 crystals) contained consecutive frames belonging to the same crystal and therefore were assigned 'multi-hit'. The number of reflections assigned just within the multi-hit dataset resulted in a completeness of 8.3% (Table 1). Due to the low completeness of the multi-hit data, complete structure determination was not possible. Therefore, a direct comparison of the electron density maps could not be carried out in the present case. An analysis of the resolution of the diffraction data associated with the 315 multi-hit crystals is presented in Figure 5B. This plot represents an analysis of the average intensity as a function of multi-hit image number from 1 to a maximum of 42 multi-hit images. The plot indicates that on average Frames 1–15 consistently contain diffraction out to a maximum resolution of ∼1.8 Å. After Frame 15, the resolution of the diffraction data declines, dropping to ∼2.1 Å by Frame 42. This clearly indicates that the decrease in resolution for the multi-hit crystals is most probably a result of sustained radiation-induced damage. Based on our analysis, we estimate that the inclusion of multiple hits in the structure analysis results in an approximately 20% decrease in the total number of crystals required for structure solution. We note that in the case of this experiment the multi-hits formed a relatively small percentage of the whole dataset and hence their inclusion or exclusion was not found to have a measurable impact on the overall quality of the data.

Table 1. Data collection statistics. Statistics for the whole dataset are compared to a subset of the data which we classified as 'multi-hit dataset'; single crystals hit multiple times. Values for the outer shell are given in parentheses.

Data Parameters	Lysozyme *	Multi-Hit Dataset
Diffraction source	Australian Synchrotron	Australian Synchrotron
Photon Energy (mean value, eV)	13,000	13,000
Flux (photons/s)	2.4×10^{12}	2.4×10^{12}
Wavelength (Å)	1.05	1.05
Temperature (°K)	300	300
Detector	Dectris EIGER X 16M	Dectris EIGER X 16M
Beam size (W,H μm)	12×22	12×22
Space group	$P4_32_12$	$P4_32_12$
a, b, c (Å)	76.68, 76.68, 38.48	76.68, 76.68, 38.48
α, β, γ, (°)	90, 90, 90	90, 90, 90
Resolution range (Å)	78.68–1.83 (2.05–1.83)	34–2.2 (7.96–2.2)
Total number frames	224,200	4389
No. of crystals	4794	315
No. total reflections	1,394,451	18,191 (2267)
No. of unique reflections	6614	1294 (159)
Completeness (%)	99.44 (99.15)	8.30 (7.9)
Redundancy	73.97 (51.34)	14.06 (11.0)
I/ σ (I)	5.08 (1.30)	3.30 (1.54)
$CC_{1/2}$	0.96 (0.47)	0.90 (0.68)
CC *	0.99 (0.81)	0.99 (0.8)
R_{split}	14.09 (93.57)	14.52 (63.71)

* These results are reproduced from Berntsen et.al. [10] with permission of AIP Publishing.

4. Discussion

Serial synchrotron crystallography provides an efficient means of generating room temperature structures using large numbers of single crystals. Whilst the technique is now routine at XFEL facilities, there is still significant development yet to be undertaken at synchrotrons. Although still at a comparatively early stage in development, SSX has already been demonstrated at a number of synchrotron facilities worldwide [10–13,15,16,19,20,49]. One of the primary motivations behind the development of injector-based SSX at synchrotrons is the possibility of conducting room temperature studies of structural dynamics—experiments which are inaccessible to cryo-EM.

In the context of molecular movies generated using TR-SX, the multi-hits we observe with our HVI could be exploited to aid in tracking structural changes from the same crystal over time. For example, if a reaction takes place over a time-period of 10–100 ms (e.g., protein folding and unfolding), then data points from the same crystal could be collected 10 ms apart (full frame, 100 Hz) or even quicker if using a region of interest (ROI) on the detector. In terms of the number of crystals required, to generate a molecular movie of just 10 frames would necessitate a 10-fold increase in the crystal volume assuming each crystal only generates one diffraction pattern. Based on the current dataset for lysozyme, this could mean that >40,000 individual crystals would need to be measured in order to generate 6000 unique reflections per time point. Either by calculation of the absorbed dose using a suitable program, e.g., RADDOSE 3D, or by performing a short calibration experiment, the threshold for radiation damage could be determined for the sample a priori and hence the flow rate of the injector could be optimised to collect the most number of hits per crystal whilst remaining below the radiation damage threshold.

The first challenge with performing SSX experiments to exploit or avoid multiple hits is to determine a method of rapidly identifying single crystals which have been measured more than once. Whilst we focus on multi-hit serial crystallography in the

context of SSX in this paper, we note that there are also potential benefits to applying this approach at XFELs. For example, multiple hits at XFEL sources have been observed in both goniometer-based SFX [50] as well as with acoustic injectors used for drop-on-demand experiments [51]. Whilst there are some key differences between SFX and SSX, particularly in terms of the pulse structure and radiation-induced damage, there are clear benefits to developing some of the concepts outlined in this paper for SSX in the context of XFELs. However, multiple hits, on the same crystal, are generally not observed in serial femtosecond crystallography (SFX) conducted at XFELs due to the destruction of the sample with each X-ray pulse [7] and have thus not previously been investigated in detail. In the present case, although Whirligig [45] provided a simple means of identifying crystal diffraction patterns having similar (<2 degree rotational difference) orientation, it does not distinguish between different crystals, therefore two consecutive crystals close together in the stream could potentially have a similar enough orientation that they could be mistaken for the same crystal. To eliminate this possibility, a second filtering step was introduced, using both the consecutive frame numbers and data collection time-stamps to confirm the images identified as 'multi-hits' are in fact from the same single crystal. As a final check, the analysis also took into account the transit time for each crystal to make sure that this was consistent with the HVI flow rate and X-ray beam size. Further examination of the multi-hit diffraction images isolated from a single crystal revealed that the Bragg reflections exhibit small rotational changes as the crystal moves through the beam which is what you would expect to see as a result of the crystal slowly tumbling as it moves with the sample stream (Movies S1–S3). The protocol we established to identify multi-hits could be used to either exclude frames which belong to the same single crystal for proteins which are highly sensitive to radiation damage in order to improve the data quality—in which case the stream speed could potentially be increased or the data simply ignored. Conversely, it could be used to optimise the number of multi-hits per crystal to help reduce crystal consumption for proteins which have a limited source or to perform time-resolved experiments on the same single crystal. Another promising application for this technique is that it could be used to study samples that are usefully perturbed via interaction with the X-ray beam. For example, single crystal spectroscopy could benefit from an optimised multi-hit SSX arrangement in order to study processes such as enzyme kinetics [52]. Based on the results from this experiment, it was estimated that it is possible to reduce the number of crystals required for a dataset by 20% via optimisation of the experimental conditions, which would enable us to collect multiple hits for every crystal. For TR-SSX studies, this increase in data volume for the same number of crystals could be critical, significantly reducing the time and cost of experiments. We also note that the protocols established for multi-hit crystallography in this paper could be particularly useful in the context of laboratory-based laser-driven ultrafast X-ray sources. In this case, the kilohertz repetition rate combined with the comparatively low flux of these sources, recently demonstrated using the EIGER detector [53], are optimal for observing and exploiting multiple hits on single crystals.

Whilst it is desirable to maximise the amount of data collected per crystal in SSX, the potential effects of radiation damage are of concern. Many factors determine whether or not radiation damage to the crystal will be noticeable in the measured diffraction data. These include the size of the crystal and the flow rate (and hence the amount of time the crystal spends in the beam), as well as the flux and beam size. In addition to this, the specific protein being investigated can also substantially alter a crystals tolerance to radiation damage, particularly if the structure has 'damage hot spots', e.g., metal centres or disulphide bonds. Generally, the literature suggests that the recommended global dose limits for proteins crystals at room temperature is around two orders of magnitude lower than that for crystals measured under cryogenic conditions. For lysozyme, the radiation dose limit is specified as 0.38 MGy [48] for room temperature versus 30 MGy for cryo-cooled crystals [54,55]. The literature also states that there is possibly no way to distinguish between the effects of global and specific radiation damage effects at room

temperature [56]. However, it is important to note that radiation dose limits are related to the specific resolution of the structure retrieval and size of the crystal. Based on the published radiation dose limits and the RADDOSE-3D calculations (Figure 2), under the conditions used in our experiment, for a crystal to maintain an absorbed dose below the radiation damage threshold and survive undamaged as it passes through the X-ray beam, it would need to have a diameter of 30 μm or greater. Given that the majority of crystals measured in this experiment fall within the 10–20 μm size range, the crystals are expected to show signs of radiation damage after 8–15 consecutive frames. This behaviour is confirmed by the observed loss in diffraction intensity which occurs in the higher resolution shells once this threshold in the number of multi-hit images is reached. Comparing the first and last images in the crystal series (Figures S1 and S2 and Table S1), there are clear signs of a loss of high resolution diffraction consistent with radiation damage occurring. However, we did find an exception to this in Crystal 1 (Figure 3 and Movie S1). This particular dataset showed no obvious reduction in Bragg peak intensities as the crystal moved through the beam likely indicating these diffraction data were collected from an outlier larger diameter crystal and hence able to tolerate a larger dose. Whilst additional experiments would be required to experimentally confirm the radiation damage limit for lysozyme using Lipidico, the results are an indication that high-resolution structural data can be generated from multiple hits whilst remaining below the radiation damage threshold. For much smaller, micron-sized, crystals using more tightly focussed X-ray beams, the number of multiple hits that are possible whilst remaining below the damage threshold are likely to be far fewer than in the present experiment. In addition, for crystals within this small size range, the effects of photoelectron escape will have an even larger impact on the radiation damage behaviour.

5. Conclusions

The occurrence of multi-hits in SSX was explored in the context of the Australian Synchrotron Lipidico injector. For high-viscosity injectors at synchrotron sources using high-frame rate detectors, the appearance of multiple hit crystals in any given dataset is highly likely. Whilst some experimentalists may want to optimise the set up to minimise the number of multi-hit diffraction patterns in their data, due to the possibility of radiation damage impacting the data quality, there is also an opportunity to exploit these multi-hit crystals, both to reduce the amount of sample required for structure retrieval and to study structural dynamics occurring on timescales on the order of 10–100 ms (depending on the frame rate of the detector). In the current experiment using crystals with a diameter primarily between 10 and 20 μm, the maximum number of measurements that could occur prior to radiation damage occurring was 8–15. Depending on the crystal size, desired resolution and beam intensity, this number could be readily increased or decreased simply by changing the flow rate.

Supplementary Materials: The following are available online at www.mdpi.com/xxx/s1, Table S1: Tracking the number of a Bragg peaks in higher resolution shells for three different crystals. The first frame, middle frame and last frame of the crystal diffraction are compared. Figure S1: Diffraction images collected from Crystal 2 over a duration of 42 consecutive images. Three images are isolated from this series: (A) Image 1, first image; (B) Image 20, middle image; and (C) Image 42, last image in the series. The red ring indicates the diffraction limit of the data. Figure S2: Diffraction images collected from Crystal 3 over a duration of 18 consecutive images. Two images were isolated from this series: (A) Image 1, first image; and (B) Image 18, last image in the series. The red ring indicates the outer resolution limit of diffraction pattern. Movie S1: Diffraction images from Crystal 1 collected over a duration of 19 consecutive images. The movie shows the diffraction pattern consistently present to high resolution limit of the data as it tumbles through the X-ray beam. Movie S2: Diffraction images collected from Crystal 2 over a duration of 42 consecutive images. Three images are isolated from this series: (A) Image 1, first image; (B) Image 20, middle image; and (C) Image 42, last image in the series. The red ring indicates the diffraction limit of the data. Movie S3: Diffraction images from

Crystal 3 collected over a duration of 18 consecutive images. The movie shows the diffraction pattern gradually changing as it tumbles through the X-ray beam.

Author Contributions: Conceptualisation, C.D., and B.A.; methodology, P.B. and C.D.; software, P.B. M.H.-J.; formal analysis, B.A., P.B., H.M., M.H.-J. and C.D.; investigation, M.H.-J., P.B., B.A. and C.D.; data curation, P.B. and M.H.-J.; writing—original draft preparation, C.D., P.B. and M.H.-J.; writing—review and editing, B.A. and C.D.; visualisation, P.B., B.A. and C.D.; supervision, B.A. and C.D.; and funding acquisition, B.A. All authors have read and agreed to the published version of the manuscript.

Funding: This work was supported by the Australian Research Council Centre of Excellence in Advanced Molecular Imaging (CE140100011) (http://www.imagingcoe.org/). M.H.-J. was also supported by ANSTO funding.

Acknowledgments: This research was undertaken in part using the MX2 beamline at the Australian Synchrotron, part of ANSTO and the beamline scientists and made use of the Australian Cancer Research Foundation (ACRF) detector. We also like to acknowledge those who were involved with the initial data collection and Mick Kusel for the design and engineering of the injector system, Lipidico.

Conflicts of Interest: The authors declare no conflict of interest.

Abbreviations

The following abbreviations are used in this manuscript:

SSX	Serial synchrotron Crystallography
WC	Whole Crystal
TR-SSX	Time resolved-serial synchrotron crystallography
SFX	Serial Femtosecond Crystallography
XFEL	X-ray Free Electron Laser

References

1. Mueller, C.; Marx, A.; Epp, S.; Zhong, Y.; Kuo, A.; Balo, A.; Soman, J.; Schotte, F.; Lemke, H.; Owen, R.; et al. Fixed target matrix for femtosecond time-resolved and in situ serial micro-crystallography. *Struct. Dyn.* **2015**, *2*, 054302. [CrossRef]
2. Gao, Y.; Xu, W.; Shi, W.; Soares, A.; Jakoncic, J.; Myers, S.; Martins, B.; Skinner, J.; Liu, Q.; Bernstein, H.; et al. High-speed raster-scanning synchrotron serial microcrystallography with a high-precision piezo-scanner. *J. Synchrotron Radiat.* **2018**, *25*, 1362–1370. [CrossRef]
3. Boutet, S.; Lomb, L.; Williams, G.J.; Barends, T.R.M.; Aquila, A.; Doak, R.B.; Weierstall, U.; DePonte, D.P.; Steinbrener, J.; Shoeman, R.L.; et al. High-Resolution Protein Structure Determination by Serial Femtosecond Crystallography. *Science* **2012**, *337*, 362–364. [CrossRef] [PubMed]
4. Suga, M.; Akita, F.; Hirata, K.; Ueno, G.; Murakami, H.; Nakajima, Y.; Shimizu, T.; Yamashita, K.; Yamamoto, M.; Ago, H.; et al. Native structure of photosystem II at 1.95 angstrom resolution viewed by femtosecond X-ray pulses. *Nature* **2015**, *517*, 99–265. [CrossRef] [PubMed]
5. Wiedorn, M.O.; Oberthur, D.; Bean, R.; Schubert, R.; Werner, N.; Abbey, B.; Aepfelbacher, M.; Adriano, L.; Allahgholi, A.; Al-Qudami, N.; et al. Megahertz serial crystallography. *Nat. Commun.* **2018**, *9*, 4025. [CrossRef] [PubMed]
6. Yefanov, O.; Oberthur, D.; Bean, R.; Wiedorn, M.O.; Knoska, J.; Pena, G.; Awel, S.; Gumprecht, L.; Domaracky, M.; Sarrou, I.; et al. Evaluation of serial crystallographic structure determination within megahertz pulse trains. *Struct. Dyn.* **2019**, *6*. [CrossRef]
7. Chapman, H.N.; Fromme, P.; Barty, A.; White, T.A.; Kirian, R.A.; Aquila, A.; Hunter, M.S.; Schulz, J.; DePonte, D.P.; Weierstall, U.; et al. Femtosecond X-ray protein nanocrystallography. *Nature* **2011**, *470*, 73–81. [CrossRef]
8. Tenboer, J.; Basu, S.; Zatsepin, N.; Pande, K.; Milathianaki, D.; Frank, M.; Hunter, M.; Boutet, S.; Williams, G.J.; Koglin, J.E.; et al. Time-resolved serial crystallography captures high-resolution intermediates of photoactive yellow protein. *Science* **2014**, *346*, 1242–1246. [CrossRef]
9. Aquila, A.; Hunter, M.S.; Doak, R.B.; Kirian, R.A.; Fromme, P.; White, T.A.; Andreasson, J.; Arnlund, D.; Bajt, S.; Barends, T.R.M.; et al. Time-resolved protein nanocrystallography using an X-ray free-electron laser. *Opt. Express* **2012**, *20*, 2706–2716. [CrossRef]
10. Berntsen, P.; Hadian-Jazi, M.; Kusel, M.; Martin, A.V.; Ericsson, T.; Call, M.J.; Trenker, R.; Roque, F.G.; Darmanin, C.; Abbey, B. The serial millisecond crystallography instrument at the Australian Synchrotron incorporating the "Lipidico" injector. *Rev. Sci. Instruments* **2019**, *90*, 085110. [CrossRef]
11. Beyerlein, K.R.; Dierksmeyer, D.; Mariani, V.; Kuhn, M.; Sarrou, I.; Ottaviano, A.; Awel, S.; Knoska, J.; Fuglerud, S.; Jonsson, O.; et al. Mix-and-diffuse serial synchrotron crystallography. *IUCrJ* **2017**, *4*, 769–777. [CrossRef] [PubMed]

12. Gati, C.; Bourenkov, G.; Klinge, M.; Rehders, D.; Stellato, F.; Oberthuer, D.; Yefanov, O.; Sommer, B.P.; Mogk, S.; Duszenko, M.; et al. Serial crystallography on in vivo grown microcrystals using synchrotron radiation. *IUCrJ* **2014**, *1*, 87–94. [CrossRef] [PubMed]
13. Martin-Garcia, J.M.; Conrad, C.E.; Nelson, G.; Stander, N.; Zatsepin, N.A.; Zook, J.; Zhu, L.; Geiger, J.; Chun, E.; Kissick, D.; et al. Serial millisecond crystallography of membrane and soluble protein microcrystals using synchrotron radiation. *IUCrJ* **2017**, *4*, 439–454. [CrossRef] [PubMed]
14. Nogly, P.; James, D.; Wang, D.J.; White, T.A.; Zatsepin, N.; Shilova, A.; Nelson, G.; Liu, H.G.; Johansson, L.; Heymann, M.; et al. Lipidic cubic phase serial millisecond crystallography using synchrotron radiation. *IUCrJ* **2015**, *2*, 168–176. [CrossRef] [PubMed]
15. Schneider, T.R.; Bourenkov, G.; Gati, C.; Chapman, H.N.; Redecke, L.; Zander, U.; Marquez, J.A.; Cipriani, F.; Schneider, T.R. Serial synchrotron crystallography experiments at EMBL beamline P14 at PETRA III. *Acta Crystallogr. Found. Adv.* **2015**, *71*, S12. [CrossRef]
16. Stellato, F.; Oberthuer, D.; Liang, M.; Bean, R.; Gati, C.; Yefanov, O.; Barty, A.; Burkhardt, A.; Fischer, P.; Galli, L.; et al. Room temperature macromolecular serial crystallography using synchrotron radiation. *IUCrJ* **2014**, *1*, 204–212. [CrossRef]
17. Meents, A.; Wiedorn, M.; Srajer, V.; Henning, R.; Sarrou, I.; Bergtholdt, J.; Barthelmess, M.; Reinke, P.; Dierksmeyer, D.; Tolstikova, A.; et al. Pink-beam serial crystallography. *Nat. Commun.* **2017**, *8*, 1281. [CrossRef]
18. Botha, S.; Nass, K.; Barends, T.R.M.; Kabsch, W.; Latz, B.; Dworkowski, F.; Foucar, L.; Panepucci, E.; Wang, M.; Shoeman, R.L.; et al. Room-temperature serial crystallography at synchrotron X-ray sources using slowly flowing free-standing high-viscosity microstreams. *Acta Crystallogr. Sect. D* **2015**, *71*, 387–397. [CrossRef]
19. Aumonier, S.; Santoni, G.; Gotthard, G.; von Stetten, D.; Leonard, G.A.; Royant, A. Millisecond time-resolved serial oscillation crystallography of a blue-light photoreceptor at a synchrotron. *IUCrJ* **2020**, *7*, 728–736. [CrossRef]
20. Weinert, T.; Skopintsev, P.; James, D.; Dworkowski, F.; Panepucci, E.; Kekilli, D.; Furrer, A.; Brunle, S.; Mous, S.; Ozerov, D.; et al. Proton uptake mechanism in bacteriorhodopsin captured by serial synchrotron crystallography. *Science* **2019**, *365*, 61. [CrossRef]
21. Schulz, E.; Mehrabi, P.; Mueller-Werkmeister, H.M.; Tellkamp, F.; Jha, A.; Stuart, W.; Persch, E.; Gasparo, R.; Diederich, F.; Pai, E.; et al. The hit-and-return system enables efficient time-resolved serial synchrotron crystallography. *Nat. Methods* **2018**, *15*. [CrossRef] [PubMed]
22. Mehrabi, P.; Schulz, E.; Agthe, M.; Horrell, S.; Bourenkov, G.; von Stetten, D.; Leimkohl, J.P.; Schikora, H.; Schneider, T.; Pearson, A.; et al. Liquid application method for time-resolved analyses by serial synchrotron crystallography. *Nat. Methods* **2019**, *16*. [CrossRef] [PubMed]
23. Mehrabi, P.; Schulz, E.; Dsouza, R.; Mueller-Werkmeister, H.M.; Tellkamp, F.; Miller, R.J.D.; Pai, E.F. Time-resolved crystallography reveals allosteric communication aligned with molecular breathing. *Science* **2019**, *365*, 1167–1170. [CrossRef] [PubMed]
24. Lee, D.; Baek, S.; Park, J.; Lee, K.; Kim, J.; Lee, S.J.; Chung, W.K.; Lee, J.L.; Cho, Y.; Nam, K.H. Nylon mesh-based sample holder for fixed-target serial femtosecond crystallography. *Sci. Rep.* **2019**, *9*. [CrossRef]
25. Martin, A.V.; Kozlov, A.; Berntsen, P.; Roque, F.G.; Flueckiger, L.; Saha, S.; Greaves, T.L.; Conn, C.E.; Hawley, A.M.; Ryan, T.M. Fluctuation X-ray diffraction reveals three-dimensional nanostructure and disorder in self-assembled lipid phases. *Commun. Mater.* **2020**, *1*, 1–8.
26. Roedig, P.; Vartiainen, I.; Duman, R.; Panneerselvam, S.; Stube, N.; Lorbeer, O.; Warmer, M.; Sutton, G.; Stuart, D.I.; Weckert, E.; et al. A micro-patterned silicon chip as sample holder for macromolecular crystallography experiments with minimal background scattering. *Sci. Rep.* **2015**, *5*. [CrossRef]
27. Shelby, M.; Gilbile, D.; Grant, T.; Seuring, C.; Segelke, B.; He, W.; Evans, A.; Pakendorf, T.; Fischer, P.; Hunter, M.; et al. Fixed Target Delivery for Serial Femtosecond Crystallography of Weakly-Diffracting Objects. *Protein Sci.* **2019**, *28*, 109–110.
28. Abbey, B.; Dilanian, R.A.; Darmanin, C.; Ryan, R.A.; Putkunz, C.T.; Martin, A.V.; Wood, D.; Streltsov, V.; Jones, M.W.M.; Gaffney, N.; et al. X-ray laser-induced electron dynamics observed by femtosecond diffraction from nanocrystals of Buckminsterfullerene. *Sci. Adv.* **2016**, *2*. [CrossRef]
29. Martiel, I.; Müller-Werkmeister, H.M.; Cohen, A.E. Strategies for sample delivery for femtosecond crystallography. *Acta Crystallogr. Sect. D* **2019**, *75*, 160–177. [CrossRef]
30. Mehrabi, P.; Müller-Werkmeister, H.M.; Leimkohl, J.P.; Schikora, H.; Ninkovic, J.; Krivokuca, S.; Andriček, L.; Epp, S.W.; Sherrell, D.; Owen, R.L.; et al. The HARE chip for efficient time-resolved serial synchrotron crystallography. *J. Synchrotron Radiat.* **2020**, *27*, 360–370. [CrossRef]
31. Conrad, C.E.; Basu, S.; James, D.; Wang, D.J.; Schaffer, A.; Roy-Chowdhury, S.; Zatsepin, N.A.; Aquila, A.; Coe, J.; Gati, C.; et al. A novel inert crystal delivery medium for serial femtosecond crystallography. *IUCrJ* **2015**, *2*, 421–430. [CrossRef] [PubMed]
32. Park, J.; Park, S.; Kim, J.; Park, G.; Cho, Y.; Nam, K.H. Polyacrylamide injection matrix for serial femtosecond crystallography. *Sci. Rep.* **2019**, *9*. [CrossRef] [PubMed]
33. Sugahara, M.; Song, C.Y.; Suzuki, M.; Masuda, T.; Inoue, S.; Nakane, T.; Yumoto, F.; Nango, E.; Tanaka, R.; Tono, K.; et al. Oil-free hyaluronic acid matrix for serial femtosecond crystallography. *Sci. Rep.* **2016**, *6*. [CrossRef] [PubMed]
34. Sugahara, M.; Mizohata, E.; Nango, E.; Suzuki, M.; Tanaka, T.; Masudala, T.; Tanaka, R.; Shimamura, T.; Tanaka, Y.; Suno, C.; et al. Grease matrix as a versatile carrier of proteins for serial crystallography. *Nat. Methods* **2015**, *12*, 61–63. [CrossRef] [PubMed]
35. Kovácsová, G.; Grünbein, M.L.; Kloos, M.; Barends, T.R.M.; Schlesinger, R.; Heberle, J.; Kabsch, W.; Shoeman, R.L.; Doak, R.B.; Schlichting, I. Viscous hydrophilic injection matrices for serial crystallography. *IUCrJ* **2017**, *4*, 400–410. [CrossRef] [PubMed]

36. Sugahara, M.; Nakane, T.; Masuda, T.; Suzuki, M.; Inoue, S.; Song, C.; Tanaka, R.; Nakatsu, T.; Mizohata, E.; Yumoto, F.; et al. Hydroxyethyl cellulose matrix applied to serial crystallography. *Sci. Rep.* **2017**, *7*, 703. [CrossRef] [PubMed]
37. Standfuss, J. Membrane protein dynamics studied by X-ray lasers—Or why only time will tell. *Curr. Opin. Struct. Biol.* **2019**, *57*, 63–71. [CrossRef]
38. DePonte, D.P.; Weierstall, U.; Schmidt, K.; Warner, J.; Starodub, D.; Spence, J.C.H.; Doak, R.B. Gas dynamic virtual nozzle for generation of microscopic droplet streams. *J. Phys. D-Appl. Phys.* **2008**, *41*. [CrossRef]
39. Oberthuer, D.; Knoska, J.; Wiedorn, M.O.; Beyerlein, K.R.; Bushnell, D.A.; Kovaleva, E.G.; Heymann, M.; Gumprecht, L.; Kirian, R.A.; Barty, A.; et al. Double-flow focused liquid injector for efficient serial femtosecond crystallography. *Sci. Rep.* **2017**, *7*. [CrossRef]
40. Ganan-Calvo, A.M. Generation of steady liquid microthreads and micron-sized monodisperse sprays in gas streams. *Phys. Rev. Lett.* **1998**, *80*, 285–288. [CrossRef]
41. Zhu, L.; Weierstall, U.; Cherezov, V.; Liu, W. Serial Femtosecond Crystallography of Membrane Proteins. *Next Gener. Membr. Protein Struct. Determ.* **2016**, *922*, 151–160.
42. Berntsen, P.; Sharma, R.; Kusel, M.; Abbey, B.; Darmanin, C. Lipidico Injection Protocol for Serial Crystallography Measurements at the Australian Synchrotron. *J. Vis. Exp.* **2020**. [CrossRef] [PubMed]
43. Schneider, C.A.; Rasband, W.S.; Eliceiri, K.W. NIH Image to ImageJ: 25 years of image analysis. *Nat. Methods* **2012**, *9*, 671–675. [CrossRef] [PubMed]
44. Hadian-Jazi, M.; Messerschmidt, M.; Darmanin, C.; Giewekemeyer, K.; Mancuso, A.P.; Abbey, B. A peak-finding algorithm based on robust statistical analysis in serial crystallography. *J. Appl. Crystallogr.* **2017**, *50*, 1705–1715. [CrossRef]
45. White, T.A.; Kirian, R.A.; Martin, A.V.; Aquila, A.; Nass, K.; Barty, A.; Chapman, H.N. CrystFEL: A software suite for snapshot serial crystallography. *J. Appl. Crystallogr.* **2012**, *45*, 335–341. [CrossRef]
46. Dickerson, J.L.; McCubbin, P.T.N.; Garman, E.F. RADDOSE-XFEL: Femtosecond time-resolved dose estimates for macromolecular X-ray free-electron laser experiments. *J. Appl. Crystallogr.* **2020**, *53*, 549–560. [CrossRef]
47. Marman, H.; Darmanin, C.; Abbey, B. The Influence of Photoelectron Escape in Radiation Damage Simulations of Protein Micro-Crystallography. *Crystals* **2018**, *8*, 267. [CrossRef]
48. de la Mora, E.; Coquelle, N.; Bury, C.S.; Rosenthal, M.; Holton, J.M.; Carmichael, I.; Garman, E.F.; Burghammer, M.; Colletier, J.P.; Weik, M. Radiation damage and dose limits in serial synchrotron crystallography at cryo- and room temperatures. *Proc. Natl. Acad. Sci. USA* **2020**, *117*, 4142–4151. [CrossRef]
49. Nogly, P.; Panneels, V.; Nelson, G.; Gati, C.; Kimura, T.; Milne, C.; Milathianaki, D.; Kubo, M.; Wu, W.; Conrad, C.; et al. Lipidic cubic phase injector is a viable crystal delivery system for time-resolved serial crystallography. *Nat. Commun.* **2016**, *7*. [CrossRef]
50. Cohen, A.E.; Soltis, S.M.; González, A.; Aguila, L.; Alonso-Mori, R.; Barnes, C.O.; Baxter, E.L.; Brehmer, W.; Brewster, A.S.; Brunger, A.T.; et al. Goniometer-based femtosecond crystallography with X-ray free electron lasers. *Proc. Natl. Acad. Sci. USA* **2014**, *111*, 17122–17127. [CrossRef]
51. Roessler, C.; Agarwal, R.; Allaire, M.; Alonso-Mori, R.; Andi, B.; Bachega, J.; Bommer, M.; Brewster, A.; Browne, M.; Chatterjee, R.; et al. Acoustic Injectors for Drop-On-Demand Serial Femtosecond Crystallography. *Structure* **2016**, *24*, 631–640. [CrossRef] [PubMed]
52. Pearson, A.; Owen, R. Combining X-ray crystallography and single-crystal spectroscopy to probe enzyme mechanisms. *Biochem. Soc. Trans.* **2009**, *37*, 378–381. [CrossRef] [PubMed]
53. Khakurel, K.P.; Espinoza, S.; Savko, M.; Polovinkin, V.; Dohnalek, J.; Shepard, W.; Angelova, A.; Hajdu, J.; Andreasson, J.; Angelov, B. Kilohertz Macromolecular Crystallography Using an EIGER Detector at Low X-ray Fluxes. *Crystals* **2020**, *12*, 1146. [CrossRef]
54. Southworth-Davies, R.J.; Medina, M.A.; Carmichael, I.; Garman, E.F. Observation of decreased radiation damage at higher dose rates in room temperature protein crystallography. *Structure* **2007**, *15*, 1531–1541. [CrossRef] [PubMed]
55. Nave, C.; Garman, E.F. Towards an understanding of radiation damage in cryocooled macromolecular crystals. *J. Synchrotron Radiat.* **2005**, *12*, 257–260. [CrossRef] [PubMed]
56. Gotthard, G.; Aumonier, S.; De Sanctis, D.; Leonard, G.; von Stetten, D.; Royant, A. Specific radiation damage is a lesser concern at room temperature. *IUCrJ* **2019**, *6*, 665–680. [CrossRef] [PubMed]